Advancements in SERS-Based Biological Detection and Its Application and Perspectives in Pancreatic Cancer

Lei Xu[a,e§], Yujiao Xie[b,c§], Jie Lin[b,c*], Aiguo Wu[b,c*], Tianan Jiang[a,d*]

a Department of Ultrasound Medicine, The First Affiliated Hospital, Zhejiang University School of Medicine, Hangzhou, Zhejiang, 310000, China

b Ningbo Key Laboratory of Biomedical Imaging Probe Materials and Technology, Zhejiang International Cooperation Base of Biomedical Materials Technology and Application, Chinese Academy of Sciences (CAS) Key Laboratory of Magnetic Materials and Devices, Ningbo Cixi Institute of Biomedical Engineering, Zhejiang Engineering Research Center for Biomedical Materials, Ningbo Institute of Materials Technology and Engineering, Chinese Academy of Sciences, Ningbo, 315201, China

c Advanced Energy Science and Technology Guangdong Laboratory, Huizhou, 516000, China

d Zhejiang University Cancer Center, Zhejiang, Hangzhou, 310000, China

e Department of Ultrasound Medicine, Affiliated Jinhua Hospital Zhejiang University School of Medicine, Jinhua, Zhejiang, 321000, China

Acknowledgements

This work is financially supported by National Natural Science Foundation of China (No. 81971623 32025021, 31971292, 52002380), Development Project of National Major Scientific Research Instrument (No.82027803), Ningbo 3315 Innovative Teams Program (Grant No. 2019A-14-C), the member of Youth Innovation Promotion Association Foundation of CAS, China (2023310).

Conflicts of interest

The authors declare no conflict of interest.

Abstract

Surface-enhanced Raman scattering (SERS) has become an essential bio-detection technique. Due to its high sensitivity, good signal specificity, and resistance to photobleaching, SERS has been widely used in biomedical research fields such as molecular imaging, tumor diagnosis, and drug monitoring. This review focuses on the progress of SERS in biomedical applications. We first introduce the basic principle of SERS and the progress of substrate research. Then we summarize the latest research progress of SERS in drug monitoring, cell and exosome detection, tumor imaging, and detection platforms combining microfluidic and lateral flow technologies. Subsequently, the applied research of SERS in early diagnosis of pancreatic cancer and drug efficacy monitoring is described. Finally, the future development direction and possible challenges of SERS in tumor diagnosis and treatment are proposed.

Key words: SERS, pancreatic cancer, biological application, diagnosis, therapy

Introduction

1. SERS Principle and Mechanism

Surface-enhanced Raman spectroscopy (SERS) is an emerging analytical that enables the detection of single molecular weight samples and provides rich fingerprint information of the molecular structure.[1, 2] SERS enhancement mechanism mainly includes electromagnetic enhancement (EM) and chemical enhancement (CM).[3-5] The electromagnetic (EM) enhancement mechanism plays a decisive role, with an enhancement range of 10^6 to 10^9. The principle of electromagnetic enhancement is primarily based on the excitation of surface plasmon resonance (LSPR) on the surface of roughened metal nanostructures. This excitation enhances the local electromagnetic field on the metal surface, leading to an increase in the Raman scattering signal of molecules on the metal surface. [6](Fig.1a). Therefore, when the nanoparticle gap is small, a "hot spot" is formed between the particles with significant electromagnetic field enhancement due to surface plasmon coupling between the nanoparticles (Fig.1b). The "hot spot" effect is the main reason for the high detection sensitivity of SERS.[7-9] The chemical enhancement (CT) mechanism refers to the interaction and charge transfer between the probe molecule and the enhanced substrate under laser irradiation at a specific frequency. Then, the molecular polarization rate increases, subsequently increasing the Raman scattering cross-section, thus enabling a more significant

enhancement of the scattering signal[10] (Fig.1c-d). Compared to the EM mechanism, it has a much shorter scope effect on the Åm range, requiring direct adsorption or chemical binding of the reporter to the metal surface. In addition, CE provides weaker enhancement than EM, typically in the field of 10^2-10^3.[11-13]

2. SERS biological detecting substrate

The SERS effect is closely related to the substrate, and gold and silver nanoparticles are widely used as SERS active substrates because of their excellent enhancement effect on numerous molecules, simple fabrication method, and convenience of storage. However, the easy clustering of gold and silver nanoparticles and the inability of some molecules to bond with them to produce SERS properties have limited the scope of the application of precious metal SERS substrates represented by gold and silver.[14-16] The emergence of semiconductor material SERS substrates in recent years has become a popular material in the field of SERS due to its controllable and abundant ontological properties, showing a broad application prospect in both the SERS field and material domain.[17-19]

2.1 Noble metal SERS substrates

It has been found that noble metal nanoparticles such as gold and silver exhibit excellent LSPR properties in the visible-near infrared region, as their application as SERS optical substrates has attracted much attention. Wang et al. [20] prepared silver nanoparticle aggregates of different

morphologies by hydrothermal method. Silver nanoparticles with varying aggregation can be produced using Anodic Aluminum oxide (AAO) as the experimental substrate (Fig 2a). It was used as a SERS substrate for the detection of pyridine molecules. The enhancement factor of the pyridine molecule was found to be 10^7 at a concentration of 10^{-10} M, which proved that it has a good SERS enhancement effect. Although silver was the first SERS active material discovered, its biological toxicity limits the application of silver-based SERS nanoparticles in vivo. However, gold nanoparticles with excellent biostability and safety are currently the most commonly used SERS tagging cores. Sun et al.[21] prepared Au nanodisk arrays on Si substrates by combining X-ray printing with electron-beam vapor deposition (Fig 2b). They controlled the reaction conditions to regulate the nanodisk size and distribution density effectively. The results showed that the Au nanodisk arrays were used as SERS active substrates to detect R6G probe molecules with the lowest detection limit of 10^{-8} M and the SERS enhancement factor of 10^6, demonstrating excellent SERS activity. The average EF of Pt and Pd substrates is 1.4×10^5, two orders of magnitude lower than that of Au/Ag and Si substrates. The detection limit of Pt/Pd substrates is also 100 times worse than that of the previously discussed Au, Ag, and Si groups, which is about 2.9×10^{-9} M[22-24]. As the research progresses, it is gradually found that the SERS enhancement effect is closely related to the composition, size, morphology, particle

spacing, and refractive index of the surrounding medium of noble metal nanoparticles.

2.2 Semiconductor SERS substrates

Recent studies have shown that semiconductor SERS substrates are economical, stable, biocompatible, and have enhanced molecular selectivity. Additionally, their physicochemical properties, such as exciton Bohr radius, energy band structure, and electron density, can be easily tuned, making them ideal materials for SERS substrates. Semiconductor SERS substrate materials encompass transition metals, metal oxides, and quantum dots. The research and development of semiconductor metal SERS substrates has significantly expanded the application of SERS technology. In a study by Zhao et al. [25] 3D Cu nanocrystals with various morphologies were fabricated on aluminum substrates. This was achieved by reducing $CuCl_2$-$2H_2O$ with glucose as the reducing agent and adjusting the surface free energy through varying the concentration of HDA. The unique 3D structures and resulting plasma coupling effect concentrated the "hot spots" at the tips and gaps of the crystals, resulting in strong SERS effects, as shown in Fig 2c. The size distribution and alignment of the 3D sword-shaped Cu nanocrystals are relatively uniform, and the enhancement factor can reach 10^7. Lin et al. [26] prepared a recrystallization-induced self-assembly (RISA) strategy to fabricate a three-dimensional cubic Cu_2O superstructure SERS substrate enriched with Cu vacancies. The presence

of Cu vacancy defects in this structure induces electrostatic adsorption and facilitates resonance coupling between the complexes, resulting in a synergistic enhancement of the charge transfer process and the SERS effect (Fig. 2d). The combined effects of Cu vacancy defects and resonance coupling significantly enhance the SERS effect. The enhancement factors (EFs) were measured at 8×8 for individual Cu_2O superconstituent particles, while for individual Cu_2O superstructure particles, the EFs reached an impressive value of 8×10^5. Moreover, the detection limits for R6G and CV molecules were notably low, at 10^{-9} M. Zhao et al. [27] synthesized MoO3-xH2O quantum dots (QDs) to achieve direct and sensitive surface-enhanced Raman spectroscopy (SERS) fingerprinting of inorganic hydrazine hydrate. The synthesized QDs, with an average size of 2.2 nm, exhibited a significant improvement in detecting hydrazine hydrate compared to larger particles of 10 and 100 nm. The detection limit of the QDs was approximately 4×10^{-5} M, reducing the minimum detectable concentration by at least 1000 times. This remarkable enhancement in SERS activity can be attributed to the quantum size effect induced by the small particle size, which is below the Bohr radius.

3. Biomedical Applications of SERS Detection

3.1 SERS Detection for CTCs

CTCs (circulating tumor cells) are present in the blood and can be an essential reference for early tumor diagnosis. However, CTCs are usually

extremely rare in peripheral blood (1 ml of blood contains a few CTCs). In addition, the presence of large numbers of leukocytes (10^7) and erythrocytes ($\sim 5\times10^9$) can interfere with CTC measurements. Therefore, the development of sensitive CTC assays is essential. Wu et al. reported composite nanoparticles with SERS functionality constructed from gold nanoparticles of different shapes (spheres, stars, rods) that can be used for the sensitive detection of CTCs.[28] To further optimize the detection capability of SERS in complex environments, the group also developed a CTC analysis system based on triangular silver nanoprisms (AgNPR) and superparamagnetic iron oxide nanoparticles (SPION).[29] The system can conduct CTCs capture, enrichment, detection, and release functions (Fig.3a). Cancer cells such as ovarian, kidney, breast, and lung cancers with high folate expression can be targeted by constructing folate receptor-targeting SERS nanoparticles. The method's detection limit can be as low as one cell per ml. In addition, by adding excess free folate receptors, the enriched CTCs can also be released for further cell expansion, phenotype identification, and molecular analysis.

3.2 SERS Detection for Exosomes

Exosomes are small vesicles secreted by cells that appear in body fluids, such as blood, urine, and saliva. Compared to traditional invasive histopathological biopsies, exosomes offer the advantage of being cost-effective and minimally invasive in disease diagnosis, treatment, and

monitoring.[30, 31] To effectively detect exosomes, the researchers have approached this in two ways.[32] One is to develop excellent SERS substrates to enhance the signal-to-noise ratio of single-molecule Raman spectroscopy. The other is to develop SERS labels modified with specific recognition elements to enhance the SERS response of the target. Sivashanmugan et al. reported bimetallic nano-plasma gap-mode SERS substrates to study exosomes. Gold nanorods (AuNRs) and silver nanocubes (AgNCs) formed a strong plasma cavity effect.[33] The use of optimized bimetallic nanoplasma gap-mode SERS substrates allows the detection of exosomes at concentrations 10^4-10^5 times lower than normal blood samples. To evaluate patient response to anti-PD-L1/PD-1 immunotherapy, Xiao et al. developed a simple and rapid procedure for quantifying exosomal PD-L1 biomarkers from clinical serum samples (Fig.3b).[34] Using Fe_3O_4@TiO_2 nanoparticles, exosomes could be enriched and isolated from solution in less than 5 min with a capture efficiency of 96.5%. After anti-PD-L1 antibody-modified SERS labels are prepared, exosomal PD-L1 can be accurately quantified in 4 μL of undiluted serum with a detection limit as low as 1 PD-L1 exosome/μL. In addition, the assay process is significantly shorter and can be completed in less than 40 minutes. Analysis based on the SERS intensity score of each sample allows differentiation between patients with early and advanced non-small cell lung cancer as well as healthy populations.

3.3 SERS Detection for drugs

In the field of life sciences and public safety, monitoring drug abuse is highly dependent on the quantitative analysis of various drug molecules. A reliable SERS method for the detection of mephedrone by preparing gold and silver nanoparticles in combination with Fractional Factorial Design showed that the relative standard deviation of the mephedrone-specific Raman peak was as low as 0.51%. The LOD was estimated to be approximately 1.6 μg/mL (9.06×10^{-6} M), allowing rapid and simple in situ detection.[35] Usually, the target sample is dispersed in a complex mixture with impurities, which poses a great challenge for the detection of drugs, especially for trace analytes.[36] SERS technology integrates single molecule sensitivity and fingerprinting features of molecular vibrations with high resistance to interference and therefore holds great promise for detecting complex samples.[37] In recent years, the SERS technique has become an excellent surface analysis tool for the detection of drugs in urine, saliva, or blood.[38, 39] For example, methamphetamine can be effectively detected using a microfluidic device that can diffuse the sample in saliva into a designated area, while significant SERS signal enhancement can be achieved by introducing a salt solution to promote the aggregation of silver nanoparticles.[40] A novel liquid interface SERS platform for detecting drugs in urine is illustrated (Fig.3c).[41] Cyclohexane (CYH) is used as the extraction solvent to extract drugs from urine with high extraction rates and

less interference from impurities. CYH as the organic phase induces large-scale self-assembly of gold nanoparticle (GNP) arrays at the CYH/water interface. Self-directed arrays at the interface of two immiscible phases allow the detection of dispersed analytes such as methamphetamine (MAMP) and 3, 4-methylenedioxy-methamphetamine (MDMA) in both oil and water-soluble phases. The application of SERS detection has been greatly developed through the multiplex detection of such ultra-trace analytes and the two-phase dual analyte detection.

3.4 SERS Imaging

3.4.1 SERS Imaging for *in vitro* experiment

Confocal Raman microscopy enables high-resolution cellular imaging based on biomolecules and has been widely used to obtain three-dimensional information. Due to the extremely low SERS signal of endogenous biomolecules, monitoring and imaging is usually performed with the help of Raman signaling molecules. These Raman signaling molecules can be adsorbed onto small-sized SERS substrates, engulfed by cells, or immobilized on the surface. In one study, the authors prepared gold nanoparticles of approximately 42 nm, modified with a near-infrared laser-sensitive Raman dye and a cell-penetrating peptide.[42] Such a system not only ensures that cells are successfully captured but also successfully images cells without photobleaching effects, as shown in Fig.4a. The Fig.4b Shows the imaging results for different cellular components of

targeted cells at other incubation times, demonstrating the promising applications of SERS imaging encoded by Raman signaling molecules. To increase the spectral stability of cellular imaging, Wu developed a semiconducting black TiO_2 nanoparticle (B-TiO_2) with significant SERS activity.[43] By constructing a B-TiO_2 bioprobe targeting cancer cells to collect SERS profiles, rapid imaging of breast cancer cells can be achieved to meet the requirements for early screening and diagnosis of cancer cells.

3.4.2 SERS Imaging for *in vivo* experiment

During tumor removal, imaging of the removed tissue is required to identify residual tumors at the margins and guide its complete removal. The feasibility of using SERS probes to detect single biomarkers after local staining of isolated mouse tissue with targeted gold-silica nanoparticles for 1 hour has been demonstrated.[44] To further explore multiplex imaging of isolated tissues by SERS, a variety of antibody-modified NPs were stained against various tumor xenografts. As shown in Fig. 4c, the multiple tumors were clearly distinguishable for imaging and EGFR and HER-2 expression showed excellent quantitative agreement with the corresponding flow cytometry results ($R > 0.98$).[45] In addition to cell imaging and tissue imaging, the application of in vivo imaging is also an important exploration of SERS technology. To assess the multiplexed in vivo imaging capabilities of the constructed SERS probes, five SERS nanotags with less spectral overlap (S420, S421, S440, S466, and S470) were injected into

mice via the tail vein. As the particles are taken up by Kupffer cells of the reticuloendothelial system, accumulation in the liver can be observed and deep tissue multiplexing can be assessed. As can be seen in Fig.4d, different SERS markers yield different imaging brightness, which informs the choice of in vivo imaging. [46] The imaging technique correlates with the spectral stability of the designed SERS tag, the Raman signal enhancement capability and biocompatibility. Exploring the construction of stable and excellent SERS probes will be an important prerequisite for broadening imaging applications.

3.5 Integrated SERS detection platform

3.5.1 Lateral Flow Platforms for SERS Detection

The application of SERS sensing technology in lateral flow test strips has also received attention, which also called paper-based microfluidics. A typical test strip contains four main structures, namely a sample pad, a conjugate pad, a nitrocellulose membrane, and an absorbent pad. There are two lines on the nitrocellulose membrane, referred to as the test and control lines. During the test, a liquid sample solution is dropped onto the sample pad, which is carried into the absorbent pad. During this process, the sample will bind to the conjugate (usually an antibody) in the conjugate pad. Finally, the bound target complexes will be captured at the test line and the others will reach the control line.[47] In a study on the detection of disease-related markers, Zhao et al. proposed a lateral flow assay (LFA)

based on core-shell SERS nanotags for the multiplexed and quantitative detection of cardiac biomarkers for the early diagnosis of acute myocardial infarction (Fig.5a).[48] Nile blue A was embedded as a reporter molecule in silver-core and gold-shell nanoparticles (NPs) that collectively form the SERS label (Ag^{NBA}@Au). Three test lines were used in the strips to detect three cardiac biomarkers, Myo, cTnI, and CK-MB. The authors noted that the amplified signal of the SERS nanotags (antibody-conjugated Ag^{NBA}@Au) and the high surface area to volume ratio (SVR) of the porous nitrocellulose membrane enabled ultra-sensitive quantification of protein markers down to as low as 0.55 pg/mL^{-1} of protein markers. This combined SERS-LFA is ultra-sensitive, fast, cost effective and easy to use, while eliminating the need for sample pre-treatment and specialist technicians.

3.5.2 Microfluidic Platforms for SERS Detection

Microfluidics, also known as lab-on-a-chip, is a technology that integrates macro-reactors on tiny devices, having the advantages of Low sample consumption, short reaction time, high detection efficiency, and high portability. Usually, the volume of biological reactions is small, which has facilitated the development of microfluidics in the field of bioanalysis. For SERS assays, the combination with the microfluidic platform can significantly improve detection efficiency and enable point-of-care. In a diagnostic study (Fig.5b), the authors developed a method to isolate plasma exosomes using microfluidics and analyze various exosome biomarkers

using SERS technology to diagnose osteosarcoma.[49] The microfluidic device based on tangential flow filtration allows for efficient separation of exosomes from cell supernatants and plasma samples. Properly designed SERS probes based on protein biomarkers achieve detection limits as low as two exosomes per microliter. Combined with multivariate statistical analysis, this enables differentiation between osteosarcoma patients and healthy controls with an accuracy of 95%. Combined with microfluidic SERS assays that do not require complex manipulation or expensive equipment, they hold great promise as a liquid biopsy technique for the clinical diagnosis of cancer. In addition, microfluidic-SERS technology can be used for the detection and differentiation of a wide range of cancers, such as breast cancer, cervical cancer, and prostate cancer, and has excellent potential in the field of early cancer diagnosis.[50, 51] More importantly, microfluidic-SERS technology also plays a role in point-of-care diseases such as blood glucose monitoring.[52]

4. SERS for precision diagnosis of pancreatic cancer

Pancreatic cancer (PC) has an extremely high mortality rate, with the overall 5-year survival rate is only 10%. In 2030, pancreatic cancer is estimated to be the third leading cause of cancer deaths in men and women[53, 54]. Moreover, individual mortality is expected to rise steadily over the following decades, with over 800,000 deaths predicted by 2040. These data imply that PC has become a global public health concern[55].

Surgery in the early stages of PC is the most effective way to improve patient survival. However, approximately 80% of patients are already at an advanced stage when first diagnosed. In such cases, patients cannot receive surgery treatment, while palliative therapy becomes the only option, which is the main reason for reduced survival [56, 57]. Therefore, increasing the early pancreatic cancer diagnosis rate is crucial to improving patient prognosis.

The main diagnostic methods for PC are imaging diagnosis, histological and cytological biopsy for pathology diagnosis, serum tumor marker testing, genetic diagnosis, and circulating tumor cell testing[58]. The imaging diagnosis of PC mainly includes ultrasound (US), computed tomography (CT), magnetic resonance imaging (MRI), endoscopic retrograde cholangiopancreatography (ERCP), and endoscopic ultrasonography (EUS)[59]. Although imaging diagnosis is compassionate and specific in the advanced stages of PC, it is challenging to diagnose the early stages of PC accurately. In addition, the endoscopic ultrasound-guided fine-needle aspiration (EUS-FNA) cytological pathology is a more precise method[60]. Still, it is invasive, costly, high-risk, and therefore unsuitable for early PC diagnosis. Genetic and tumor marker testing provides a non-invasive way for early PC diagnosis[61, 62]. However, genetic and tumor marker tests are mainly based on polymerase chain reaction (PCR)[63] and enzyme-linked immunosorbent assays (ELISA)[64]. Although PCR and ELISA are susceptible and specific methods, they are expensive, time-consuming and

require trained personnel and restrictive experimental conditions[65]. Therefore, finding a new way for early PC diagnosis is crucial and urgent.

Surface-enhanced Raman spectroscopy (SERS) is a non-invasive, rapid, and highly sensitive detection method[66, 67]. The technique can detect characteristic fingerprint peaks for different types of cells[68], proteins[32], miRNA[69] and DNA[70]. Therefore, SERS has unique advantages in the early diagnosis of tumors[71]. SERS offers two methodologies regarding biomedical applications, including labeled detection with Raman reporter and recognition units, and label-free detection without any tags. [72] In recent years, SERS detection results of several studies have demonstrated the great potential of SERS technology in the early diagnosis and monitoring of the therapy efficacy of PC[73, 74],as shown in table 1. It is expected to become a new detection tool in clinical practice.

4.1 Labeled SERS for the detection of PC

Due to the inherent stability and distinctiveness of the Raman spectrum peak exhibited by the reporter molecule, the Labelled SERS method commonly employs Raman reporter molecules as SERS tags for achieving ultra-sensitive detection of biomedical samples[75]. Through SERS-Tag and specific anti-bodies binding, tumor cells can be targeted for recognition and capture[76]. Simultaneously, using noble metal substrates can amplify the Raman signal emitted by captured tumor cells, thereby enabling highly sensitive diagnosis of these cells [77]. Wang et al. developed a SERS-based

sandwich immunoassay for the early diagnosis of PC[78] (Fig.6). A SERS bioprobe was prepared using gold nanoparticles, 4-nitrophenyl thiol, monoclonal anti-bodies and combined gold capture substrate to detect the tumor marker Mucin-4 (MUC-4), which was impossible to detect in PC patient sera by ELISA. The research has also found that this SERS-based sandwich immunoassay is more effective than traditional methods in detecting the classic tumor marker carbohydrate antigen 19-9 (CA 19-9) in patients' serum. Similarly, Kim et al. reported a novel multiplex immunoassay that uses gold nanoparticles, 4-Nitrobenzenethiol (4-NBT) and antibodies as a SERS bioprobe to detect the biomarkers CA19-9, matrix metalloproteinase-7 (MMP-7), and MUC4 in serum samples[79]. The innovative approach enables PC diagnosis by comparing the expression patterns of these biomarkers in PC patients, pancreatitis patients, and healthy individuals. Additionally, Marc D. Porter et al. prepared a multiplexed assay platform using gold nanoparticles and 5,5-Dithiobis(succinimidy1-2-nitrobenzoate) (DSNB) [80] (Fig.7). The result of using this platform for the detection of two serum markers specific for pancreatic cancer, serum CA19-9 and MMP7, has the following advantages over conventional ELISA: (1) it is suitable for analytical multiplexing, (2) it requires only one-tenth of the sample volume required for ELISA, (3) and has a superior limit of detection (LOD) than ELISA. To investigate the ability of SERS to detect precancerous cells. Moritz F.

Kircher et al. have developed a highly sensitive SERS bioprobe by coating gold nanostars with silica and resonant Raman reporter IR-780 perchlorate [81]. Using a mouse model of the pancreas in situ, they have effectively showcased the capability of gold nanostars SERS bioprobe and its mapping modality in precisely identifying the presence and location of pancreatic tumors, including sub-millimeter-sized tumor metastatic lesions. (Fig.8). The findings of this study also highlight the precise delineation of tumor tissue boundaries achievable through the utilization of the SERS MAPPING technique. In recent developments, SERS bioprobe have been employed for the detection of miRNA biomarkers and tumor-derived exosomes. Li et al. designed and prepared a three-dimensional array of ordered micro-nanostructures based on AgNPs as a highly sensitive SERS substrate, followed by the addition of a rapid enrichment strategy magnetic beads @ exosome @ SERS detection probe (MEDP) to form an efficient sandwich immune complex for the detection of exosomes LRG-1 and GPC-1 for the diagnosis of PC [74] (Fig.9). The MEDP @ H-SERS immunocomplex presented a robust and dependable method for early PC diagnosis, exhibiting impressive sensitivity, specificity, and area under the curve values of 91.4%, 86.7%, and 0.95 (95% confidence interval: 0.849-0.991), respectively. Pang et al. [82] have fabricated a dual SERS bioprobe using Fe_3O_4@Ag-DNA and Au@Ag@DTNB (Figure.10). The research found that this dual SERS-enhanced bioprobe could recognize low-level

single base mismatches, even at concentrations as low as 1 aM. Furthermore, this experiment showed that using this SERS bioprobe to determine microRNA-10b concentrations in patient blood samples and residual plasma supernatants makes it possible to accurately distinguish between PC, chronic pancreatitis (CP) and healthy people. Li et al. reported a sandwich structure using a "chip exosome-PEARL tag" nanostructure [83] (Fig.11). The nanostructure was formed by PDA modification of antibody reporter Ag (shell) - Au (core) multilayer (PEARL) SERS tags. This method mainly uses SERS immunosensors to target and identify migration invasion factor (MIF), a tumor biomarker highly expressed in the exosome of PC, for diagnosis. This method requires only 2 μL blood samples to diagnose and classify PC. This study result provides a new strategy for the early diagnosis and staging of PC.

4.2 Label-free SERS bioprobe for the detection of PC

The label-free SERS detecting effectively differentiates various types and subtypes of pancreatic tumor cells by analyzing the inherent spectral features of live cells[84]. However, it is currently challenging to find a simple method to extract the characteristic Raman fingerprint peaks of PC cells, thus limiting the medical application of this technique. Many attempts have been made to overcome this limitation are summarized below: Hiroaki Ito's team explored a highly sensitive method for diagnosing pancreatic tumors[85]. They placed human serum samples on phosphor bronze chips

with silver nano hexagonal columns (NHCs) and irradiated them with a low-intensity helium-neon red laser beam at 633 nm. Tumor cells were successfully identified by analyzing the SERS spectra and peak intensities of the samples. Remarkably, this method demonstrated the ability to detect tumor cells at concentrations as low as 1/1000. Subsequent experiments also confirmed that this method is effective for detecting gastrointestinal tumors. Kaur et al. [73] reported label-free detection and analysis of exosomes from normal and pancreatic cancer cells using surface-enhanced Raman spectroscopy (SERS) combined with principal component difference function analysis (PC-DFA), with Ti/Au as the substrate (Fig.12). This method utilizes label-free SERS detection in conjunction with principal component-discriminant function analysis (PC-DFA) to establish a predictive model. Through this model, the accuracy for identifying pancreatic cancer patients and healthy individuals is 87% and 90%, respectively. Lee et al.[86] developed a reliable and rapid SERS-based urine analysis platform using 3D-stacked silver nanowires (AgNWs) on a glass fibre filter (GFF) sensor (Fig.11). The platform performed label-free urine-SERS analysis to obtain spectral data, followed by unsupervised principal component analysis (PCA) and supervised orthogonal partial least squares discriminant analysis (OPLS-DA) for multivariate analysis to differentiate pancreatic tumor patients from healthy individuals. Furthermore, this study found that the detection of pancreatic cancer using

the OPLS-DA method was superior to PCA, with sensitivity and specificity reaching 100%.

4.3 SERS bioprobe for monitoring the therapeutic effect

Accurate monitoring of anti-tumor drug concentrations is crucial for effective tumor therapy. Excessive drug concentrations can lead to unnecessary harm to normal cells and severe side effects, while insufficient drug concentrations may fail to eliminate tumors effectively. In recent years, several studies have found that assessing the concentration and efficacy of anti-tumor drugs through changes in SERS signal intensity is feasible and accurate. Litti et al. [87]synthesized a new SERS-based colloidal nanosensor for monitoring the concentration of erlotinib, a drug targeted to therapy for pancreatic or lung cancer. They used erlotinib and propynyl fluorescent red (PFR), which competed with AuNP-N3, to produce a SERS signal to revealing demonstrate changes in PFR's SERS corresponding to changes in erlotinib concentration. The results of this study provide a new method and idea for detecting anti-cancer drug concentrations. Subsequently, Mukhopadhyay et al.[88] successfully developed a highly specific and sensitive DNA-SWCNT SERS bioprobe for real-time monitoring of the response of PC cells to chemotherapy drugs such as gemcitabine. The reversible alteration of the Raman G band in the carbon nanotubes within the SERS bioprobe can reflect the concentration changes of hydrogen peroxide within tumor cells. As gemcitabine functions by

generating a large amount of hydrogen peroxide to kill PC cells, the real-time changes in hydrogen peroxide concentration within PC cells can indirectly reflect the response of PC to gemcitabine. Furthermore, Sujai et al. [89] reported a photothermal therapeutic nano envelope (PTTNe: MnO2@AuNPs). This nano envelope, composed of manganese dioxide-covered gold nanoparticles (AuNPs), exhibited excellent photothermal therapeutic efficacy when exposed to 808 nm laser irradiation for killing pancreatic cancer cells (Fig.13). Notably, the therapeutic effect of photothermal therapy (PTT) could be monitored in real time by observing changes in cellular SERS signals. Evaluating tumor cell apoptosis and necrosis after PTT through changes in SERS signals within PC cells was consistent with the results obtained through flow cytometry. However, this assessment method based on changes in SERS signals requires less sample and time. It offers higher sensitivity, providing a new approach and concept for accurate real-time detection of therapeutic efficacy.

5. Conclusion and Future Perspective

In this review, we aim to provide a comprehensive overview of the recent advancements in biomedical applications of surface-enhanced Raman scattering (SERS). SERS spectroscopy is widely used in the biological field due to its advantages of high sensitivity, rapid analysis, fingerprint spectroscopy, and non-invasiveness. In tumor precise diagnosis, SERS bioprobes can accurately diagnose individual tumor cells through

labeled and label-free detection. In tumor precision therapy, the initial therapeutic effect of anti-tumor drugs can be monitored by observing the changes in the intensity and peak position of SERS fingerprint peaks. The synthesis method for PC-specific labeled SERS bioprobes is usually divided into two steps. Initially, monoclonal antibodies are attached to nanoparticles that carry reporter molecules and SERS substrates. This approach facilitates the precise targeting and capture of specific markers, forming a sandwich structure. Subsequently, the SERS signal is obtained using laser irradiation through reporter molecules on the nanoparticles, thus indirectly detecting PC cells in body fluids such as blood and urine. tumor cells often secrete or express a variety of different types of biomarkers. As a result, the detection sensitivity of a SERS biosensor increases with the ability to simultaneously identify a greater number of tumor biomarkers. Therefore, the development of a PC SERS bioprobe that combines multiple antibodies to simultaneously identify multiple biomarkers is one of the important future research directions. Kim et al. [79] have performed a preliminary study in this area, using gold nanoparticles, 4-Nitrobenzenethiol (4-NBT) and antibodies to prepare a multiplex immunoassay with LOD of 2 ng/mL^{-1} as a SERS bioprobe to accurately detect three PC biomarkers CA19-9, MMP7, and MUC4 simultaneously.

In comparison, label-free SERS detection is a direct analysis of the SERS signals of different cells to identify tumor cells from normal cells

based on the specific molecular fingerprint peaks of different cells[90]. However, the SERS signals of individual cells are not very distinct and characteristic fingerprint peaks are not obvious, so it is often necessary to combine machine learning methods to improve the sensitivity and accuracy of the test[91]. The most used machine learning methods are PCA-LDA, PC-DFA and PCA&OPLS-DA[92-94]. In addition, the composition and structure of the SERS substrate have a more significant impact on the effectiveness of the detection in label-free SERS detection than in labeled SERS detection. Currently, commonly used substrates are solid-phase and sol-gels composed of gold or silver nanoparticles. Lee et al. [86]prepared a SERS substrate for detecting pancreatic cancer cells using 3D-stacked silver nanowires and glass fibre filters. The substrate's enhancement factor (EF) was up to 1.7×10^7. Besides the material's structure, the substrate material's composition also significantly impacts the performance of the SERS detection. Currently, SERS substrates are mainly composed of gold or silver, while SERS substrates made of non-noble metal nanomaterials (e.g. C, Ti, Zn, Cu, Mo and W) offer better economy, stability, selectivity and biocompatibility than precious metal substrates. In addition, recent studies have found that semiconductor materials have good SERS performance. Li et al. [95] prepared SERS substrates of $SnSe_2$ NPAs, which demonstrated ultra-low detection limits (1×10^{-12} M), high enhancement factors (1.33×10^6), and excellent homogeneity (relative standard deviation down to

7.7%), meeting or exceeding the performance of conventional metal SERS substrates. It is one of the most sensitive semiconductor SERS substrates reported to date. However, the use of non-precious metal and semiconductor SERS substrates for detecting PC has not been reported.

Microfluidic platform-based exosome SERS detection of PC is also one of the future research hotspots.[96] Exosomes can directly reflect the fundamental information of PC cells, making them potential biomarkers for early diagnosis of PC.[97] However, due to the small size of exosomes and their relative density to body fluids, it is difficult to isolate and analyze exosomes from complex biological samples[98]. Traditional exosome isolation methods require large instruments and equipment, which are time-consuming and complicated. Microfluidics has unique advantages in terms of exosome isolation, enrichment and SERS detection, so combining the three techniques can further improve the sensitivity and accuracy of early diagnosis of PC[99]. In addition, the microfluidic technology can be used for SERS detection and analysis of single pancreatic cancer cells, laying a solid foundation for SERS detection in the pancreatic tumor microenvironment, tumor metastasis and tumor immunity.

Real-time surface-enhanced Raman-guided surgical resection of tumors is an important future medical application of Raman technology. The technique distinguishes between tumor and normal tissue by analysing in real time the specific Raman signal produced by the tumor cells themselves

or by secretions, thus delineating the tumor boundary precisely for the purpose of precise tumor removal[100] The technology has been used to conduct initial exploratory research in surgical navigation strategies for glioma Li et al. used gold nanostars to prepare a surface-enhanced resonance Raman scattering bioprobe with a PH ratiometrically response across the blood-brain barrier and proposed a novel strategy to observe acidic 'metabolic boundaries' to guide the surgery. The strategy was subsequently demonstrated in an animal glioma precision resection experiment.[101] In recent years, a seriers of studies have demonstrated that it is feasible and safe to use the endoscopic Raman systems for accurate early qualitative diagnosis and real-time tumor margin identification of gastric[102], esophageal[103] and colorectal cancers.[104] Either surgical navigation or endoscopic systems play an extremely important role in the diagnosis and treatment of PC. Hence, it is reasonable to assume that combining SERS technology with intraoperative navigation systems or SERS technology with endoscopic technology to improve the early diagnosis and survival rates of PC is feasible shortly and is one of the research directions that deserves our focused attention.

Table 1. SERS bioprobes for early detection and monitor the therapeutic effect of PC

Analysis method	Component	PC biomarker	Detection limit/ Therapy method	Sample/Model	Ref.
Labelled-SERS	AuNPs NBT	MUC4	33 ng/mL	Serum	[78]
Labelled-SERS	AuNPs-4-NBT	CA19-9, MMP7, & MUC4	2 ng/mL	Sera	[79]
Labelled-SERS	AuNPs-DSNB	MMP-7& CA19-9	MMP-7: 2.28 pg/mL; CA19-9: 34.5 pg/mL	Serum	[80]
Labelled-SERS	Au nano star-Si- IR-780 perchlorate	Precancerous Cells	1.5 fM	Serum	[81]
Labelled-SERS	MEDP @ AgNPs-DTNB & MBA	Exosome (LRG1 & GPC1)	15 particles/μL	Serum	[74]
Labelled-SERS	Fe_3O_4 @Ag-DNA-Au@Ag@DTNB	MicroRNA10a & MicroRNA10b	1 aM	Serum	[82]
Labelled-SERS	Polydopamine-encapsulate-antibody-reporter-Ag(shell)-Au(core) multilayer (PEARL)	Exosome- markers (MIF/GPC1/EGFR)	9×10^{-19} mol/L	Serum	[83]
Label-free SERS	Ag-NHCs	Histone-and-DNA complex	1/1000 of serum	Serum	[85]
Label-free SERS & PC-DFA	Ti/Au	Exosome	n/a	Serum	[73]
Label-free SERS & PCA/ OPLS-DA	AgNWs- GFF	n/a	1.7 μg/mL	Urine	[86]
Label-free SERS	AuNPs		Targeted drug therapy	Serum	[87]
SERS- Real-Time Monitoring of Therapeutic Responses	DNA-SWCNT		Chemotherapy	Vitro	[88]

SERS-guided-Real-time monitoring	MnO2@AuNPS	Photothermal Therapy	Vitro	[89]

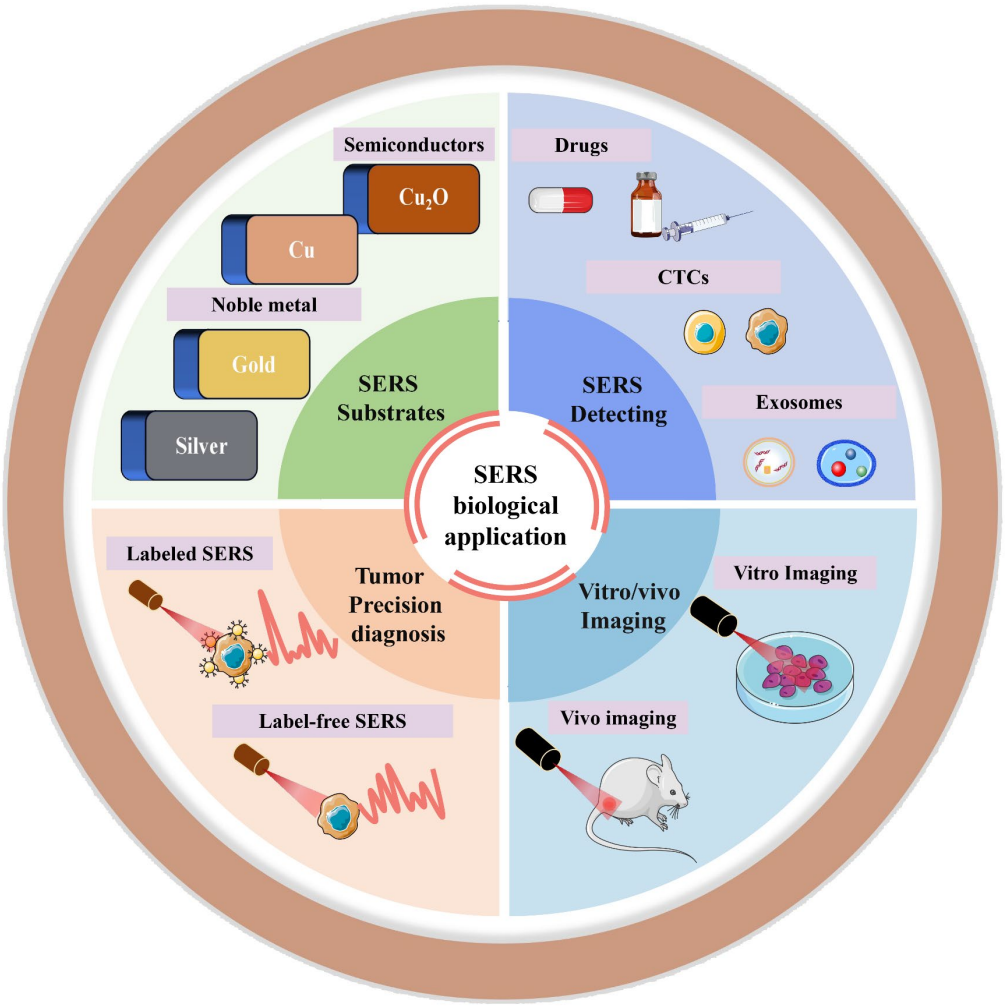
Semiconductors
Cu_2O
Cu
Noble metal
Gold
Silver
SERS Substrates
Drugs
CTCs
SERS Detecting
Exosomes
SERS biological application
Labeled SERS
Tumor Precision diagnosis
Label-free SERS
Vitro/vivo Imaging
Vitro Imaging
Vivo imaging

TOC

Figures:

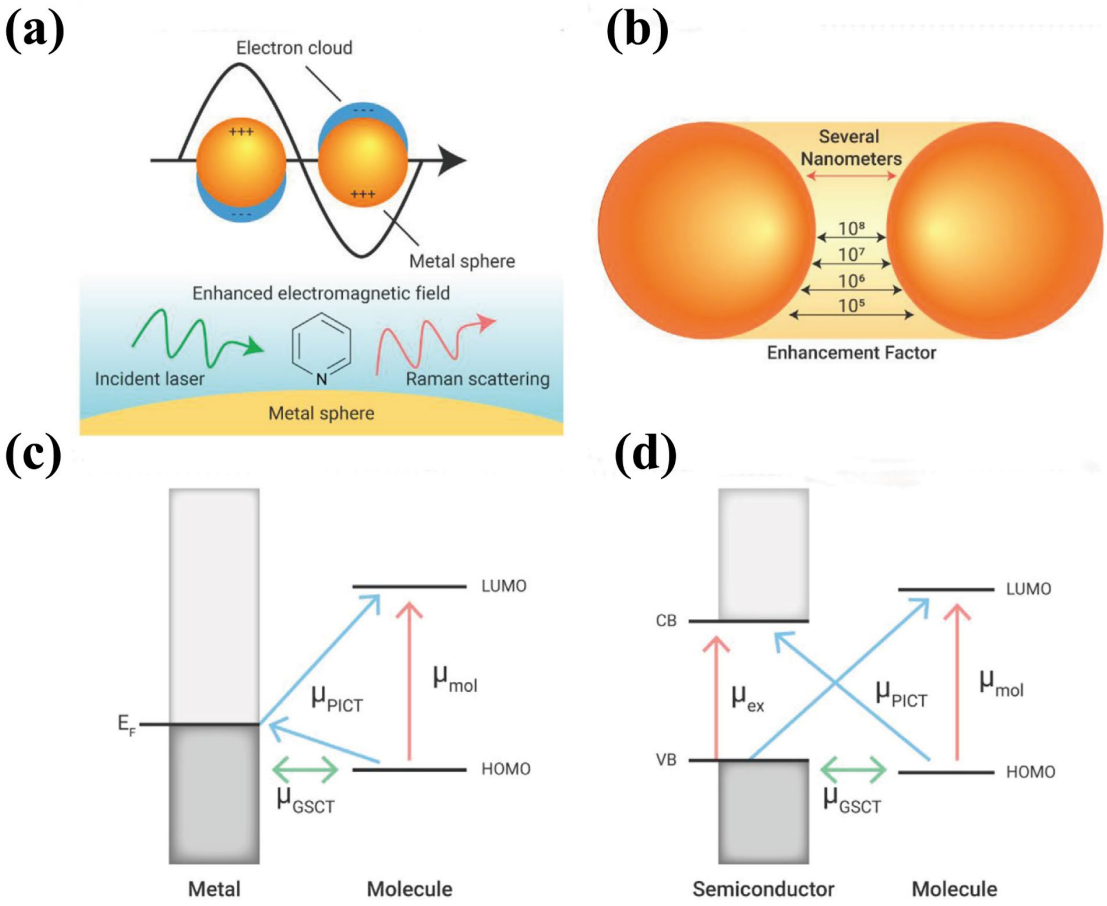

Figure 1. Electromagnetic and Chemical Mechanism for SERS Enhancement. (a) Electromagnetic enhancement in SERS based on plasmonic nanospheres. (b) Schematic illustration of a "hot spot" in the gap between adjacent particles and the corresponding change in SERS enhancement factor with relative positions. Comparison of the charge transfer transitions in a metal-molecule system (c) and a semiconductor-molecule system (d). Adapted and reproduced from ref. 5 with permission from the Elsevier Copyright 2020.

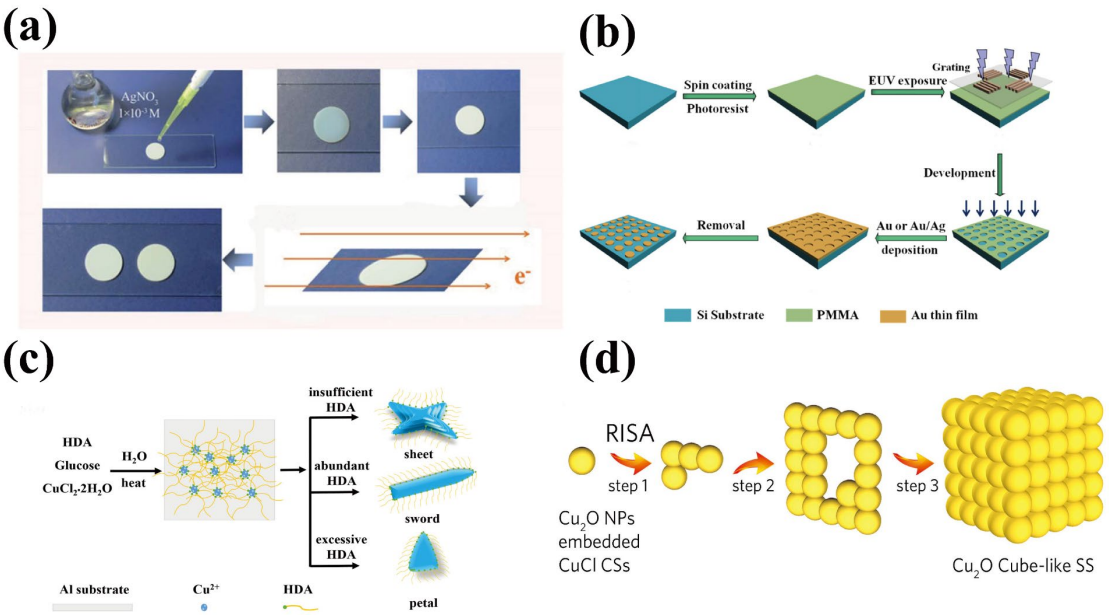

Figure 2. Examples of noble metal and semiconductor SERS substrates fabrication: (a) The synthesis process of Ag/AAO-2 substrate, adapted and reproduced from ref. 19 with permission from the Royal Society of Chemistry (RCS) Copyright 2011; (b) The fabrication process of Au or Au/Ag nanodisk array, adapted and reproduced from ref. 20 with permission from the IOP Publishing Copyright 2011; (c) Schematic illustration for the formation of Cu crystal, adapted and reproduced from ref. 24 with permission from the John Wiley and Sons Copyright 2018; (d) Self-assembly process for the formation of Cu2O cube-like superstructures, adapted and reproduced from ref. 25 with permission from the John Wiley and Sons Copyright 2016.

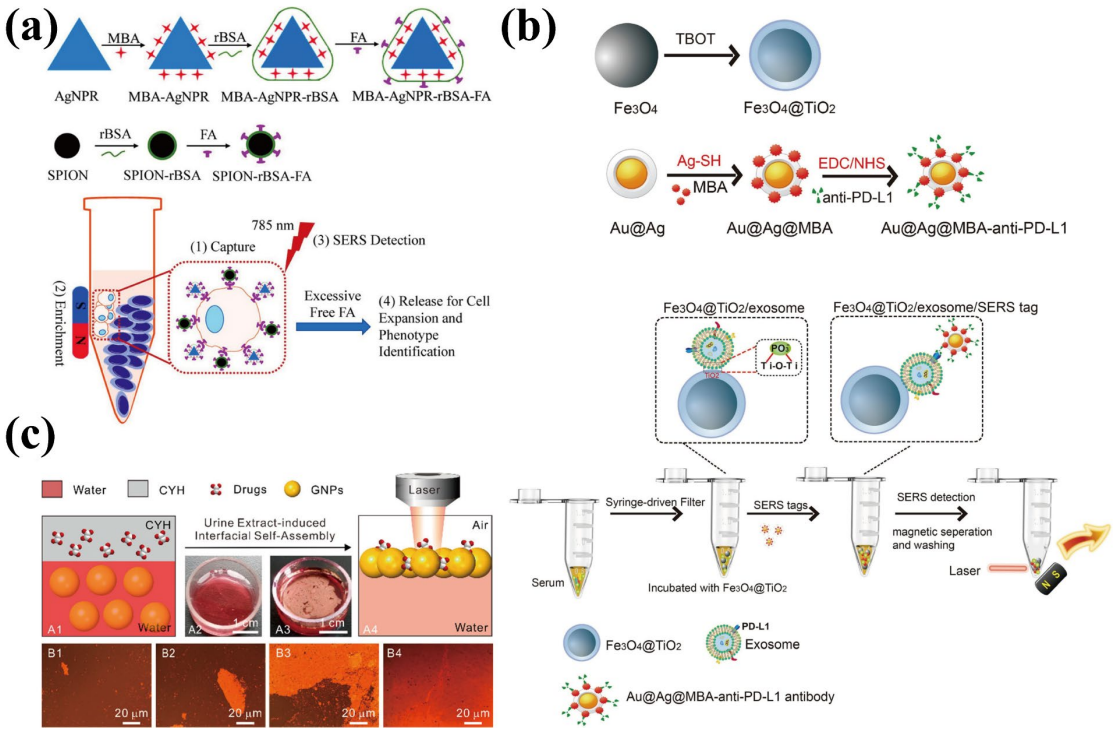

Figure 3. Example of SERS detection: (a) Schematic illustration of the designed AgNPR and SPION to form a supersensitive CTC detection SERS bioprobe, with the functions of capture, enrichment, detection, and release of CTCs in blood; Adapted and reproduced from ref. 28 with permission from the American Chemical Society (ACS) Copyright 2018. (b) Schematic view of the nanoparticles synthesis and SERS tag-based exosomal PD-L1 detection; adapted and reproduced from ref. 32 with permission from the Elsevier Copyright 2019 (c) Schematic Illustrations and Optical Images of the Urine Extract-Induced Self-Assembly of GNP Arrays at the Liquid/Air Interface for SERS Detection and Microscope Images of Self-Assembly Process of the Large-Scale Interfacial GNP Arrays; adapted and reproduced from ref. 38 with permission from the American Chemical Society (ACS) Copyright 2016.

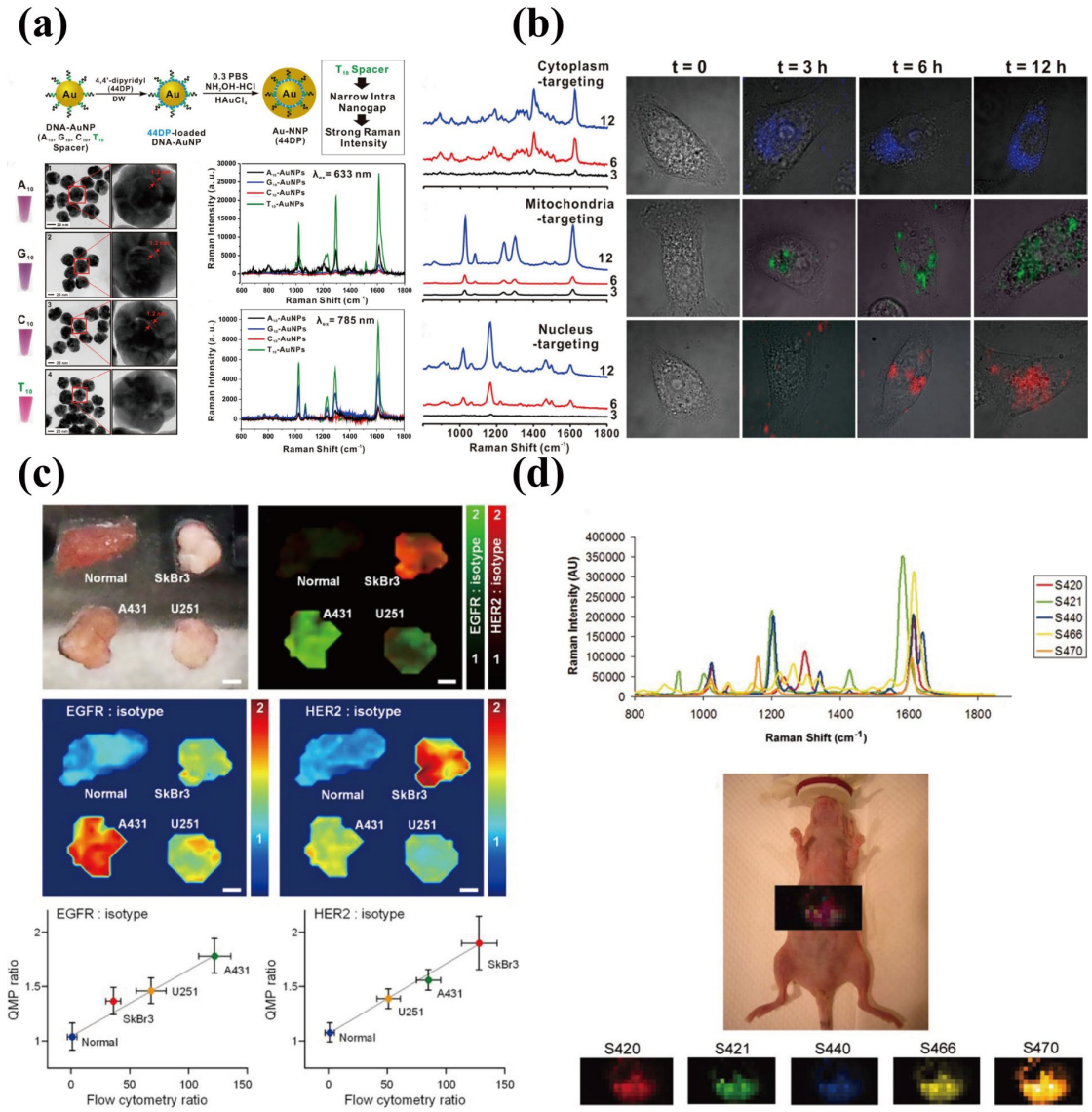

Figure 4. Examples of SERS imaging: (a) Synthetic scheme of Raman dye (44DP)-coded Au-NNPs. The solution color and HR-TEM image of 44DP-coded Au-NNPs prepared from A10 spacer DNA-AuNP, G10 spacer DNA-AuNP, C10 spacer DNA-AuNP, and T10 spacer DNA-AuNP. Raman spectra of 44DP-coded Au-NNP solution prepared from four different spacer DNA with an excitation of 633 and 785 nm; (b) Time-dependent live cell Raman images after incubating with subcellular targeting NNPs; adapted from ref. 39 with permission from American Chemical Society (ACS) Copyright 2015; (c) QMP imaging, with 0.5-mm spatial resolution, of tumor-xenograft specimens stained with a three-flavor NP mixture (EGFR-NPs, HER2-NPs and isotype-NPs); Adapted from ref. 42 with permission from Springer Nature Copyright 2016; (d) Graph depicting five unique Raman spectra, each associated with its own SERS batch: S420 (red), S421 (green), S440 (blue), S466 (yellow), and S470 (orange). Deep-tissue detection Raman image of liver overlaid on digital photo of mouse in the liver after 24 h post i.v. injection. Adapted from ref. 43 with permission from the National Academy of Sciences of the United States of America Copyright 2009.

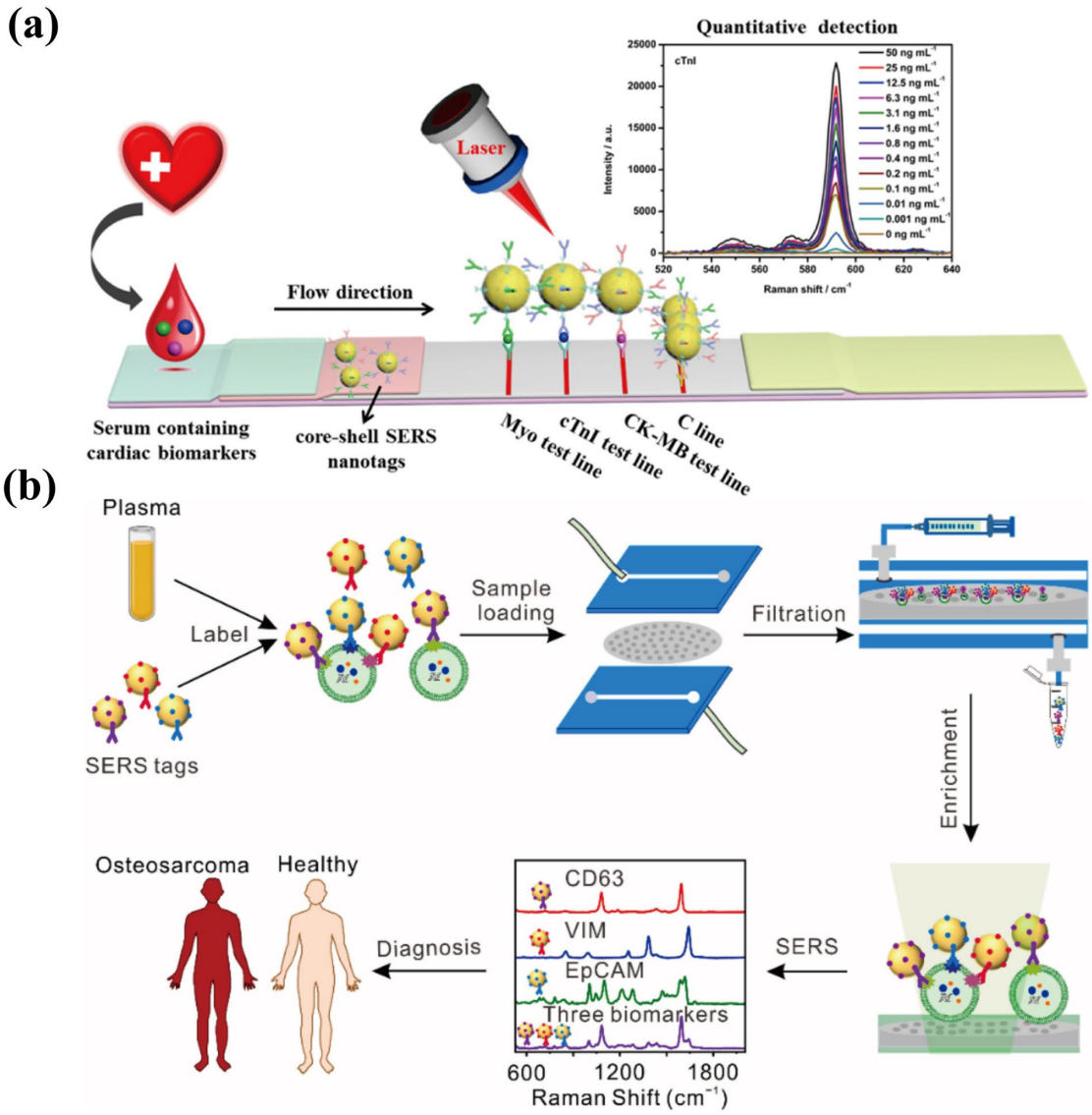

Figure 5. Example of integrated SERS detection platform (a) Schematic illustration of the core-shell SERS nanotag-based multiplex LFA. Adapted from ref. 45 with permission from the Elsevier Copyright 2018; (b) Schematic illustration of SERS profiling of three biomarkers on plasma-derived exosomes isolated by size-dependent microfluidic filtration for the diagnosis of osteosarcoma; adapted from ref. 46 with permission from the Elsevier Copyright 2022.

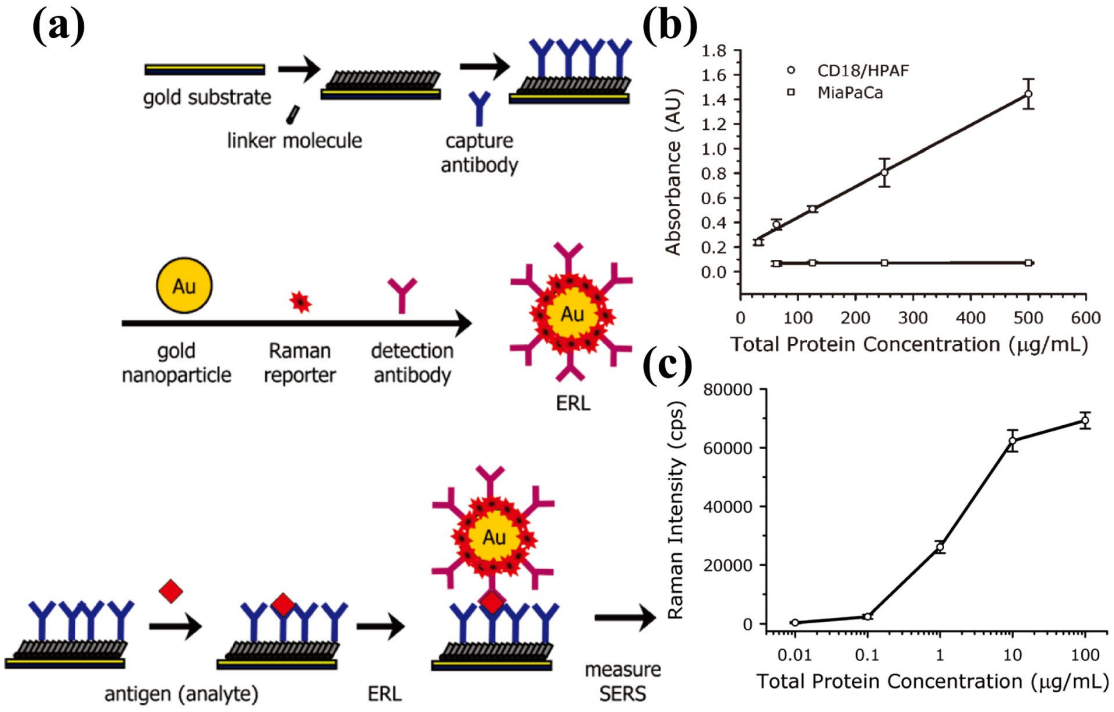

Figure 6. (a) Schematic of SERS-based immunoassay for MUC4 and CA19-9; (b) ELISA measurements of CD18/HPAF (positive control) and MiaPaCa (negative control) lysates; (c) Dose-response SERS curve for CD18/HPAF in PBS buffer. Adapted and reproduced from ref. 75 with permission from the American Chemical Society (ACS) Copyright 2011.

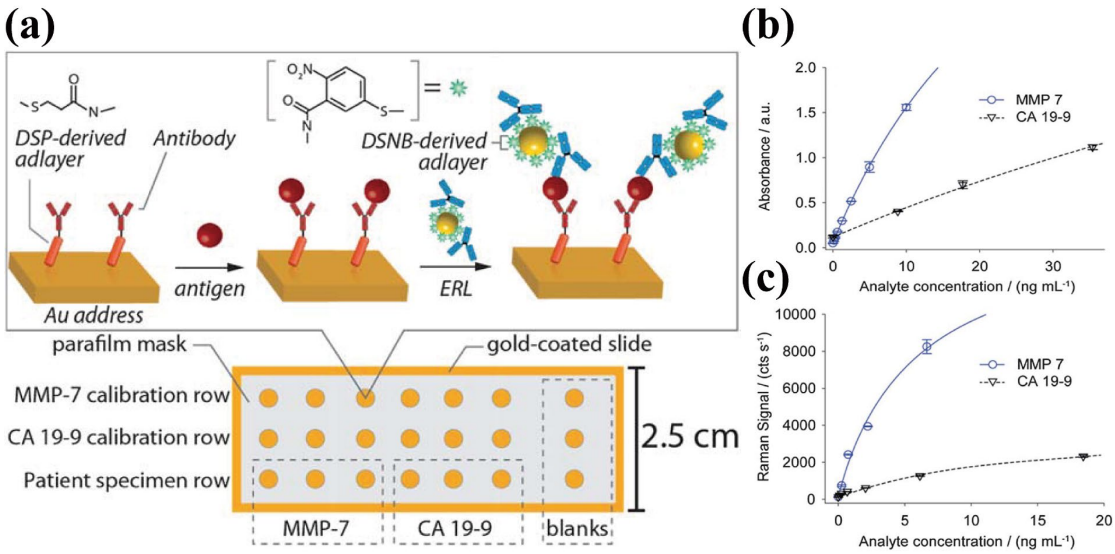

Figure 7. (a) Schematic of SERS array for MMP-7 and CA19-9;(b) ELISA calibration plots for the same MMP-7 and CA 19-9 standards used in (a); (c) SERS Calibration plots for MMP-7 and CA 19-9 antigen spiked into 1: 4 pooled human serum: PBS buffer. Adapted and reproduced from ref. 77 with permission from the Royal Society of Chemistry.

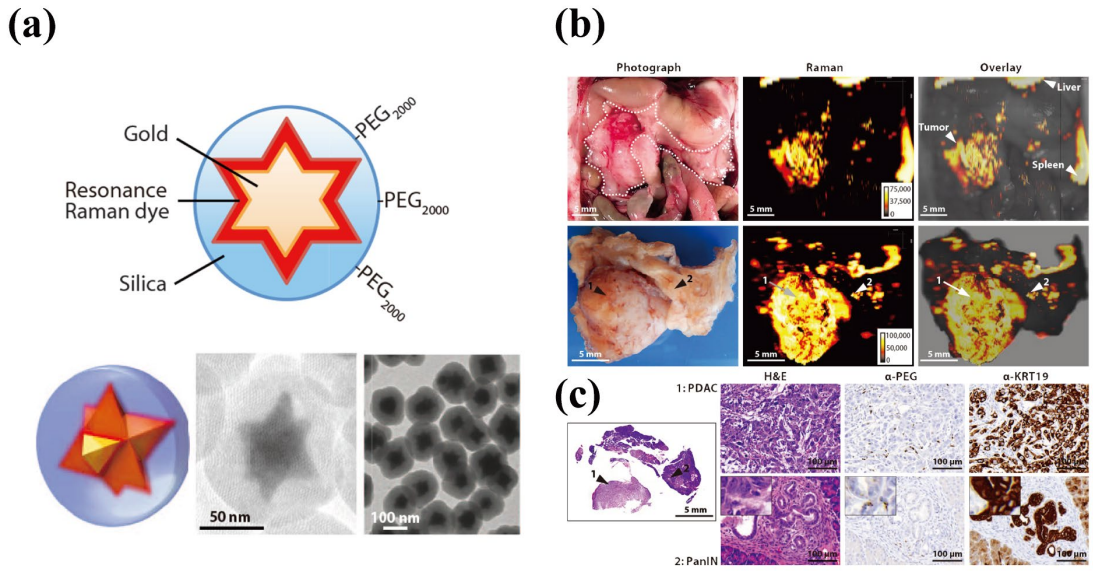

Figure 8. (a) Schematic and three-dimensional representations of the SERS nanostar geometry; Transmission electron micrographs of a single SERS nanostar and a population of SERS nanostars are shown. (b) In situ photograph and corresponding Raman images of the exposed upper abdomen in a mouse with a PDAC in the head of the pancreas and other normal-appearing regions. (c) H&E staining of the whole pancreas, including PDAC (arrow 1) and PanIN (arrow 2). Histology and keratin 19 (KRT19) staining in regions 1 and 2 confirmed lesions. Insets are 4× magnification views. Adapted and reproduced from ref. 78 with permission from the American Association for the Advancement of Science Copyright 2015.

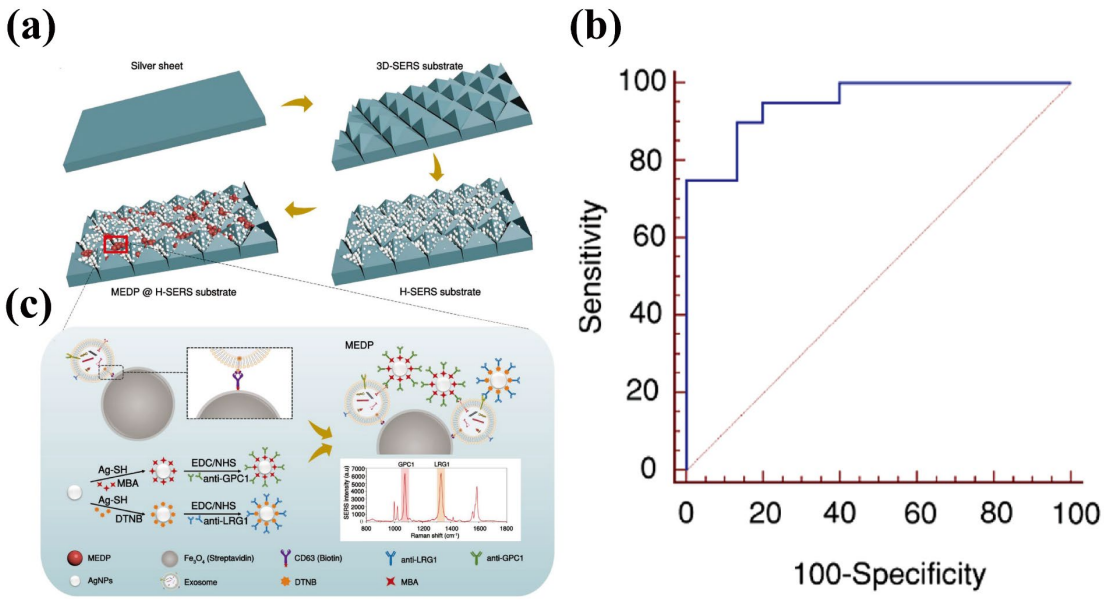

Figure 9. (a) The synthesis process of the H-SERS substrate. (b) ROC analysis to evaluate the diagnostic power of the GPC1-Exos and LRG1-Exos for the detection of early PaC; (c) Illustration of the construction of exosome capture system, the fabrication of SERS detection probes, and the SERS detection of exosomes. Adapted and reproduced from ref. 71 with permission from the John Wiley and Sons Copyright 2022.

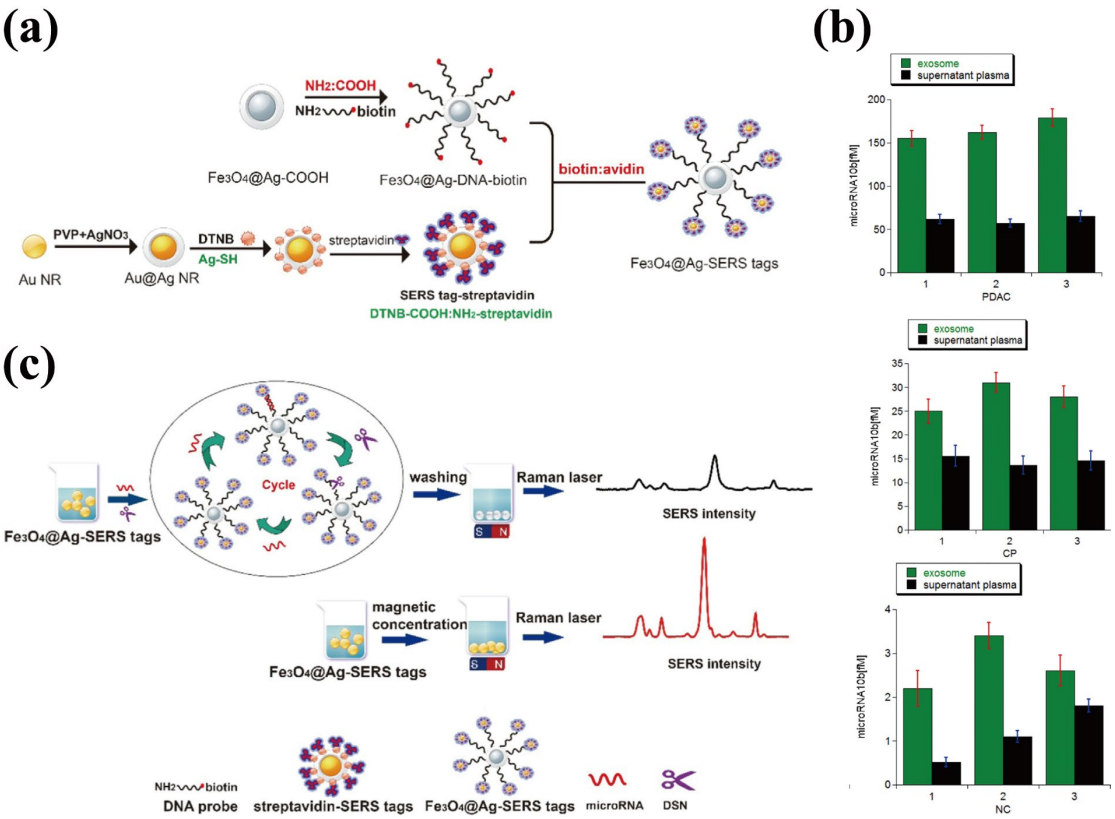

Figure 10. (a) The synthesis process of Fe3O4@Ag-SERS tags; (b) Determination of microRNA-10b concentration in exosome and residual supernatant plasma from three patients with PDAC, three normal control (NC), and three patients with CP using our SERS sensors; (c) Scheme of SERS detection of microRNA. Adapted and reproduced from ref. 79 with permission from the Elsevier Copyright 2019.

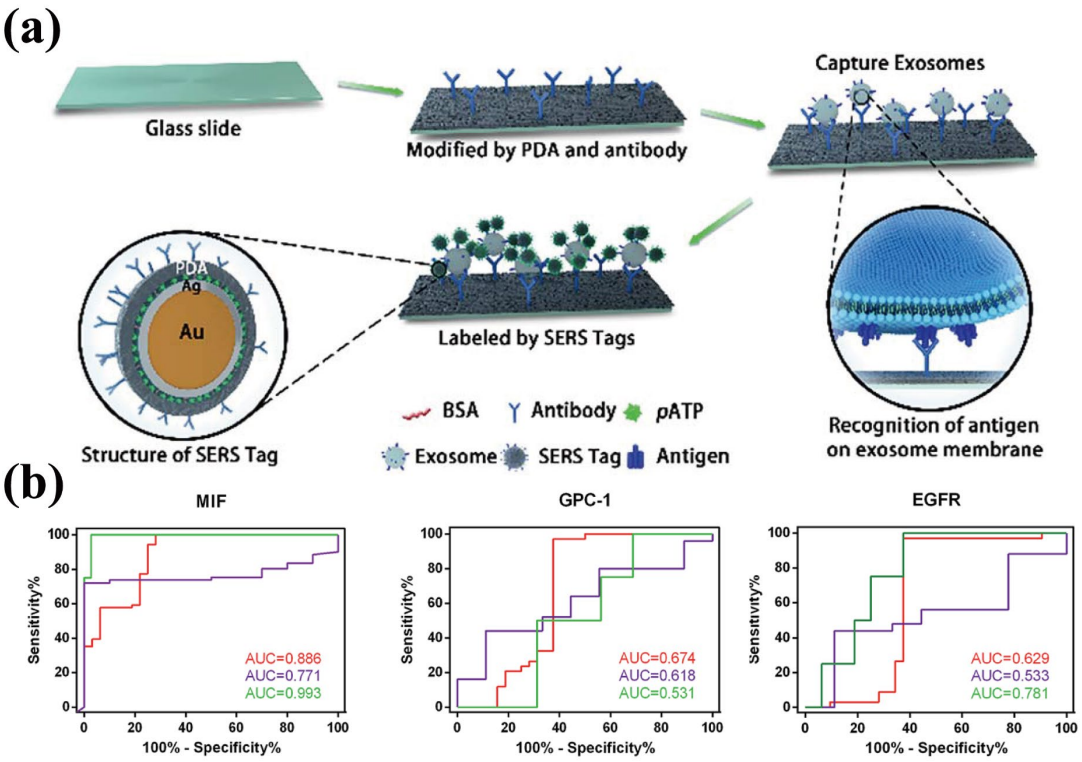

Figure 11. (a)The schematic of the PDA chip and PEARL SERS tag-based exosome sensors; (b) Receiver operating characteristic (ROC) curves were calculated for single exosome markers (MIF, GPC-1 and EGFR) (red: pancreatic cancer vs. healthy controls; purple: metastasis vs. non-metastasis; and green: P1, P2 vs. P3). AUC stands for the area under the curve. Adapted and reproduced from ref. 80 with permission from the Royal Society of Chemistry Copyright 201.

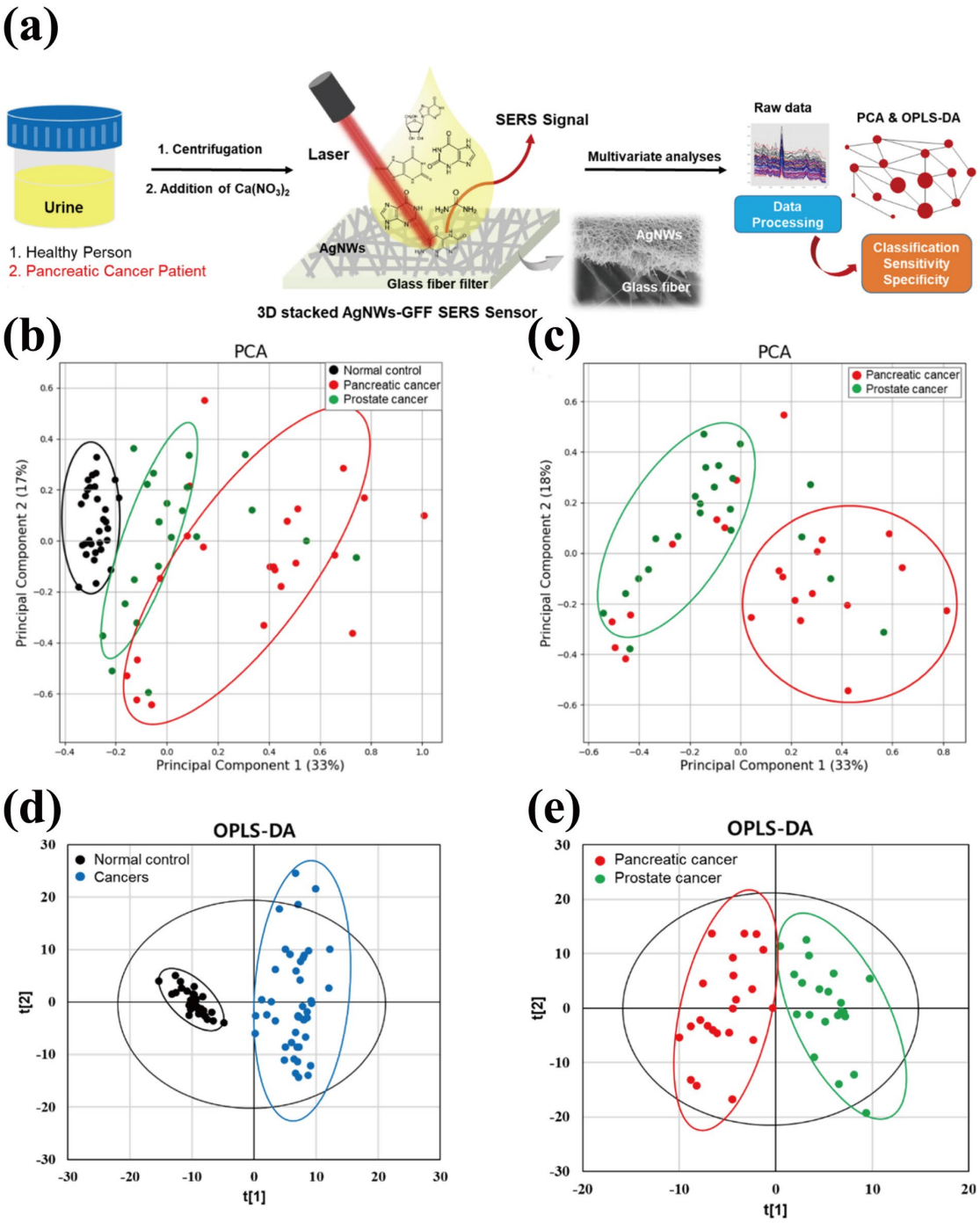

Figure 12. (a) Schematic diagram of the AgNW-GFF SERS sensor and urine analysis for the diagnosis of pancreatic cancer; PCA for (b) three groups of normal control, pancreatic cancer, and prostate cancer, and for (c) pancreatic cancer and prostate cancer; OPLS-DA for (d) classification of normal control and cancer groups and for (e) classification of pancreatic cancer and prostate cancer. Adapted and reproduced from ref. 70 with permission from the American Chemical Society (ACS) Copyright 2021.

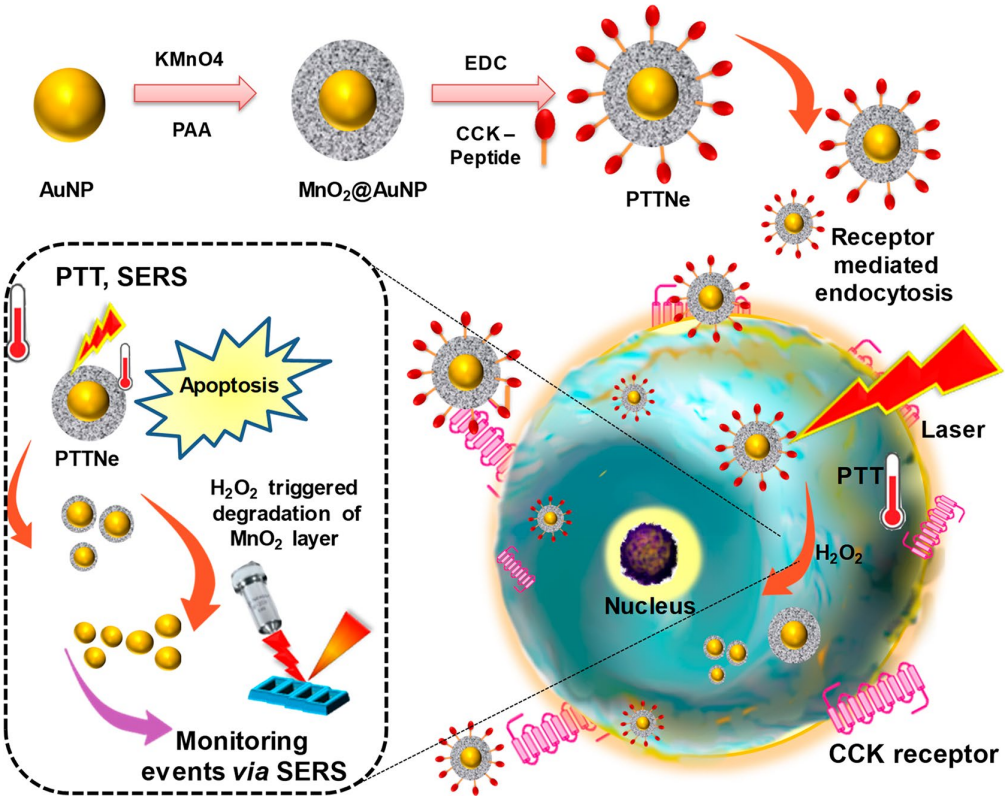

Figure 13. Schematic Representation of PTTNe as a SERS-Guided Photothermal Agent for Pancreatic Cancer. Adapted and reproduced from ref. 86 with permission from the Elsevier Copyright 2021.

Reference

1. D. L. Jeanmaire and R. P. Vanduyne, *J. Electroanal. Chem.*, **1977**, 84, 1.
2. M. G. Albrecht and J. A. Creighton, *J. Am. Chem. Soc.*, **1977**, 99, 5215.
3. M. Moskovits, *J. Chem. Phys.*, **1978**, 69, 4159.
4. W. E. Doering and S. M. Nie, *J. Phys. Chem. B*, **2002**, 106, 311.
5. S. Cong, X. Liu, Y. Jiang, W. Zhang and Z. Zhao, *Innovation*, **2020**, 1, 100051.
6. T. Itoh, K. Yoshida, H. Tamaru, V. Biju and M. Ishikawa, *J. Photochem. Photobiol., A*, **2011**, 219, 167.
7. L. F. Han, Y. J. Zhou, Z. Tan, H. T. Zhu, Y. X. Hu, X. Ma, F. Zheng, F. Feng, C. Wang and W. Y. Liu, *Anal. Chem.*, **2023**, 95, 6312.
8. G. Liman, E. Yildiz, H. Ilhan, A. E. Cetin and G. Demirel, *Adv. Opt. Mater.*, **2021**, 9.
9. P. A. Mercadal, J. C. Fraire and E. A. Coronado, *J. Phys. Chem. C*, **2022**, DOI: 10.1021/acs.jpcc.2c02299.
10. X. Meng, L. Qiu, G. Xi, X. Wang and L. Guo, *SmartMat*, **2021**, 2, 466.
11. B. Liu, B. Thielert, A. Reutter, R. Stosch and P. Lennens, *J. Phys. Chem. C*, **2019**, 123, 19119.
12. J. L. Ma, W. X. Dong, T. Xu, G. D. Wei, C. J. Gu and T. Jiang, *Analyst*, **2023**, 148, 1752.
13. D. J. Trivedi, B. Barrow and G. C. Schatz, *J. Chem. Phys.*, **2020**, 153.
14. R. Ossig, Y. H. Kwon, H. D. Kronfeldt, F. Trager and F. Hubenthal, 2012.
15. Y. Q. Cao, J. W. Zhang, Y. Yang, Z. R. Huang, N. V. Long and C. L. Fu, *Appl. Spectrosc. Rev.*, **2015**, 50, 499.
16. L. He, S. P. Mulvaney, S. K. St Angelo and M. J. Natan, *Abst. Pap. Am. Chem. Soci.*, **1998**, 216, U631.
17. X. J. Wang, E. Zhang, H. M. Shi, Y. F. Tao and X. D. Ren, *Analyst*, **2022**, 147, 1257.
18. Y. Q. Liu, Z. H. He, C. J. Ma, S. S. Zhao, J. Yan, Q. Wang and X. C. Tan, *Vib. Spectrosc.*, **2023**, 126.
19. V. S. Vendamani, R. Beeram and V. R. Soma, *J. Alloys Compd.*, **2023**, 959.
20. W. Wang, M. M. Yang, Z. Y. Wang, J. M. Yan and C. J. Liu, *Rsc Adv.*, **2014**, 4, 63079.
21. P. P. Zhang, S. M. Yang, L. S. Wang, J. Zhao, Z. C. Zhu, B. Liu, J. Zhong and X. H. Sun, *Nanotechnology*, **2014**, 25.
22. Y. Sun, R. X. Wang, X. Liu, G. Y. Shan, Y. W. Chen, T. Tong and Y. C. Liu, *Microchim. Acta*, **2018**, 185.
23. C. Y. Song, Y. Z. Sun, J. X. Li, C. Dong, J. J. Zhang, X. Y. Jiang and L. H. Wang, *Nanoscale*, **2019**, 11, 18881.
24. A. K. Verma and R. K. Soni, *Surf. Interfaces*, **2023**, 39.
25. X. H. Zhao, M. Deng, G. F. Rao, Y. C. Yan, C. Y. Wu, Y. Jiao, A. Q. Deng, C. Y. Yan, J. W. Huang, S. H. Wu, W. Chen, T. Y. Lei, P. Xu, W. D. He and J. Xiong, *Small*, **2018**, 14.
26. J. Lin, Y. Shang, X. Li, J. Yu, X. Wang and L. Guo, *Adv. Mater.*, **2017**, 29.
27. G. Song, H. Sun, J. Chen, Z. Chen, B. Liu, Z. Liu, S. Cong and Z. Zhao, *Anal. Chem.*, **2022**, 94, 5048.
28. X. Wu, Y. Xia, Y. Huang, J. Li, H. Ruan, T. Chen, L. Luo, Z. Shen and A. Wu, *ACS Appl. Mater. Interfaces*, **2016**, 8, 19928.
29. H. Ruan, X. Wu, C. Yang, Z. Li, Y. Xia, T. Xue, Z. Shen and A. Wu, *ACS Biomater. Sci. Eng.*, **2018**, 4, 1073.

30. Q. Han, L. Lv, J. Wei, X. Lei, H. Lin, G. Li, J. Cao, J. Xie, W. Yang, S. Wu, J. You, J. Lu, P. Liu and J. Min, *Cancer Lett.*, **2019**, 457, 47.
31. Z. Sun, Y. Jiang and M. Stenzel, *SmartMat*, **2021**, 2, 127.
32. J. Li, Y. Li, P. Li, Y. Zhang, L. Du, Y. Wang, C. Zhang and C. Wang, *Acta Biomater.*, **2022**, 144, 1.
33. K. Sivashanmugan, W.-L. Huang, C.-H. Lin, J.-D. Liao, C.-C. Lin, W.-C. Su and T.-C. Wen, *J. Taiwan Inst. Chem. Eng.*, **2017**, 80, 149.
34. Y. Pang, J. Shi, X. Yang, C. Wang, Z. Sun and R. Xiao, *Biosens. Bioelectron.*, **2020**, 148, 111800.
35. S. Mabbott, E. Correa, D. P. Cowcher, J. W. Allwood and R. Goodacre, *Anal Chem*, **2013**, 85, 923.
36. J. He, G. Li and Y. Hu, *Anal Chem*, **2015**, 87, 11039.
37. R. Zhang, Y. Zhang, Z. C. Dong, S. Jiang, C. Zhang, L. G. Chen, L. Zhang, Y. Liao, J. Aizpurua, Y. Luo, J. L. Yang and J. G. Hou, *Nature*, **2013**, 498, 82.
38. T. Kraemer and H. H. Maurer, *J. Chromatogr. B Biomed. Sci. Appl.*, **1998**, 713, 163.
39. G. Zheng, I. Pastoriza-Santos, J. Pérez-Juste and L. M. Liz-Marzán, *SmartMat*, **2021**, 2, 446.
40. C. Andreou, M. R. Hoonejani, M. R. Barmi, M. Moskovits and C. D. Meinhart, *ACS Nano*, **2013**, 7, 7157.
41. Y. Ma, H. Liu, M. Mao, J. Meng, L. Yang and J. Liu, *Anal Chem*, **2016**, 88, 8145.
42. J. W. Kang, P. T. C. So, R. R. Dasari and D.-K. Lim, *Nano Lett.*, **2015**, 15, 1766.
43. J. Lin, W. Ren, A. Li, C. Yao, T. Chen, X. Ma, X. Wang and A. Wu, *ACS Appl. Mater. Interfaces*, **2020**, 12, 4204.
44. J. V. Jokerst, Z. Miao, C. Zavaleta, Z. Cheng and S. S. Gambhir, *Small*, **2011**, 7, 625.
45. Y. Wang, S. Kang, A. Khan, G. Ruttner, S. Y. Leigh, M. Murray, S. Abeytunge, G. Peterson, M. Rajadhyaksha, S. Dintzis, S. Javid and J. T. Liu, *Sci. Rep.*, **2016**, 6, 21242.
46. C. L. Zavaleta, B. R. Smith, I. Walton, W. Doering, G. Davis, B. Shojaei, M. J. Natan and S. S. Gambhir, *Proc. Natl. Acad. Sci. USA*, **2009**, 106, 13511.
47. Z. Huang, A. Zhang, Q. Zhang and D. Cui, *J. Mater. Chem. B*, **2019**, 7, 3755.
48. D. Zhang, L. Huang, B. Liu, H. Ni, L. Sun, E. Su, H. Chen, Z. Gu and X. Zhao, *Biosens. Bioelectron.*, **2018**, 106, 204.
49. Z. Han, X. Peng, Y. Yang, J. Yi, D. Zhao, Q. Bao, S. Long, S.-X. Yu, X.-X. Xu, B. Liu, Y.-J. Liu, Y. Shen and L. Qiao, *Biosens. Bioelectron.*, **2022**, 217, 114709.
50. Y. Wang, Q. Li, H. Shi, K. Tang, L. Qiao, G. Yu, C. Ding and S. Yu, *Lab Chip*, **2020**, 20, 4632.
51. X. Xu, J. Lin, Y. Guo, X. Wu, Y. Xu, D. Zhang, X. Zhang, X. Yujiao, J. Wang, C. Yao, J. Yao, J. Xing, Y. Cao, Y. Li, W. Ren, T. Chen, Y. Ren and A. Wu, *Biosens. Bioelectron.*, **2022**, 210.
52. H. M. Tay, S. Y. Leong, X. Xu, F. Kong, M. Upadya, R. Dalan, C. Y. Tay, M. Dao, S. Suresh and H. W. Hou, *Lab Chip*, **2021**, 21, 2511.
53. R. L. Siegel, K. D. Miller, N. S. Wagle and A. Jemal, *CA Cancer J. Clin.*, **2023**, 73, 17.
54. C. J. Halbrook, C. A. Lyssiotis, M. Pasca di Magliano and A. Maitra, *Cell*, **2023**, 186, 1729.

55. C. J. Cabasag, J. Ferlay, M. Laversanne, J. Vignat, A. Weber, I. Soerjomataram and F. Bray, *Gut*, **2022**, 71, 1686.
56. J. D. Mizrahi, R. Surana, J. W. Valle and R. T. Shroff, *Lancet*, **2020**, 395, 2008.
57. P. H. Viale, *J. Adv. Pract. Oncol.*, **2020**, 11, 135.
58. W. Park, A. Chawla and E. M. O'Reilly, *JAMA*, **2021**, 326, 851.
59. M. Al-Hawary, *J. Natl. Compr. Cancer Network*, **2016**, 14, 678.
60. S. F. Crino, R. Di Mitri, N. Q. Nguyen, I. Tarantino, G. de Nucci, P. H. Deprez, S. Carrara, M. Kitano, V. M. Shami, G. Fernandez-Esparrach, J. W. Poley, F. Baldaque-Silva, T. Itoi, E. Manfrin, L. Bernardoni, A. Gabbrielli, E. Conte, E. Unti, J. Naidu, A. Ruszkiewicz, M. Amata, R. Liotta, G. Manes, F. Di Nuovo, I. Borbath, M. Komuta, L. Lamonaca, D. Rahal, K. Hatamaru, M. Itonaga, G. Rizzatti, G. Costamagna, F. Inzani, M. Curatolo, D. S. Strand, A. Y. Wang, A. Gines, O. Sendino, M. Signoretti, L. van Driel, K. Dolapcsiev, Y. Matsunami, S. van der Merwe, H. van Malenstein, F. Locatelli, L. Correale, A. Scarpa and A. Larghi, *Gastroenterology*, **2021**, 161, 899.
61. G. Chen, D. Luo, N. Zhong, D. Li, J. Zheng, H. Liao, Z. Li, X. Lin, Q. Chen, C. Zhang, Y. Lu, Y.-T. Chan, Q. Ren, N. Wang and Y. Feng, *Front. Immunol.*, **2022**, 13.
62. I. J. M. Levink, I. J. Visser, B. D. M. Koopmann, L. M. J. W. van Driel, J. W. Poley, D. L. Cahen, M. J. Bruno and G. M. Fuhler, *Gastrointes. Endosc.*, **2022**, 96, 801.
63. C. Bettegowda, M. Sausen, R. J. Leary, I. Kinde, Y. Wang, N. Agrawal, B. R. Bartlett, H. Wang, B. Luber, R. M. Alani, E. S. Antonarakis, N. S. Azad, A. Bardelli, H. Brem, J. L. Cameron, C. C. Lee, L. A. Fecher, G. L. Gallia, P. Gibbs, D. Le, R. L. Giuntoli, M. Goggins, M. D. Hogarty, M. Holdhoff, S.-M. Hong, Y. Jiao, H. H. Juhl, J. J. Kim, G. Siravegna, D. A. Laheru, C. Lauricella, M. Lim, E. J. Lipson, S. K. N. Marie, G. J. Netto, K. S. Oliner, A. Olivi, L. Olsson, G. J. Riggins, A. Sartore-Bianchi, K. Schmidt, l.-M. Shih, S. M. Oba-Shinjo, S. Siena, D. Theodorescu, J. Tie, T. T. Harkins, S. Veronese, T.-L. Wang, J. D. Weingart, C. L. Wolfgang, L. D. Wood, D. Xing, R. H. Hruban, J. Wu, P. J. Allen, C. M. Schmidt, M. A. Choti, V. E. Velculescu, K. W. Kinzler, B. Vogelstein, N. Papadopoulos and L. A. Diaz, *Sci. Transl. Med.*, **2014**, 6, 224ra24.
64. A. M. Seifert, C. Reiche, M. Heiduk, A. Tannert, A.-C. Meinecke, S. Baier, J. von Renesse, C. Kahlert, M. Distler, T. Welsch, C. Reissfelder, D. E. Aust, G. Miller, J. Weitz and L. Seifert, *Oncogene*, **2020**, 39, 3102.
65. A. D. Singhi, E. J. Koay, S. T. Chari and A. Maitra, *Gastroenterology*, **2019**, 156, 2024.
66. S. Deng, J. Gu, Z. Jiang, Y. Cao, F. Mao, Y. Xue, J. Wang, K. Dai, L. Qin, K. Liu, K. Wu, Q. He and K. Cai, *J. Nanobiotechnol.*, **2022**, 20, 415.
67. Q. Li, H. Huo, Y. Wu, L. Chen, L. Su, X. Zhang, J. Song and H. Yang, *Adv. Sci.*, **2023**, DOI: 10.1002/advs.202202051, e2202051.
68. X. X. Han, R. S. Rodriguez, C. L. Haynes, Y. Ozaki and B. Zhao, *Nat. Rev. Methods Primers*, **2022**, 1, 87.
69. J. Kim, J. Park, J. Ki, H. W. Rho, Y.-M. Huh, E. Kim, H. Y. Son and S. Haam, *Biosens. Bioelectron.*, **2022**, 207, 114143.
70. L. Wu, A. Dias and L. Diéguez, *Biosens. Bioelectron.*, **2022**, 204, 114075.
71. W. Zhang, L. Jiang, R. J. Diefenbach, D. H. Campbell, B. J. Walsh, N. H. Packer and Y. Wang, *ACS Sens.*, **2020**, 5, 764.
72. D. Cialla-May, X. S. Zheng, K. Weber and J. Popp, *Chem. Soc. Rev.*, **2017**, 46, 3945.

73. J. Carmicheal, C. Hayashi, X. Huang, L. Liu, Y. Lu, A. Krasnoslobodtsev, A. Lushnikov, P. G. Kshirsagar, A. Patel, M. Jain, Y. L. Lyubchenko, Y. Lu, S. K. Batra and S. Kaur, *Nanomedicine*, **2019**, 16, 88.
74. J. Li, Y. Li, S. Chen, W. Duan, X. Kong, Y. Wang, L. Zhou, P. Li, C. Zhang, L. Du and C. Wang, *Small Methods*, **2022**, 6, e2200154.
75. N. Choi, H. Dang, A. Das, M. S. Sim, I. Y. Chung and J. Choo, *Biosens. Bioelectron.*, **2020**, 164, 112326.
76. Q. Zhang, R. Ma, Y. Zhang, J. Zhao, Y. Wang and Z. Xu, *ACS Sens.*, **2023**, 8, 875.
77. N. Ferreira, A. Marques, H. Águas, H. Bandarenka, R. Martins, C. Bodo, B. Costa-Silva and E. Fortunato, *ACS Sens.*, **2019**, 4, 2073.
78. G. Wang, R. J. Lipert, M. Jain, S. Kaur, S. Chakraboty, M. P. Torres, S. K. Batra, R. E. Brand and M. D. Porter, *Anal. Chem.*, **2011**, 83, 2554.
79. N. Banaei, A. Foley, J. M. Houghton, Y. Sun and B. Kim, *Nanotechnology*, **2017**, 28, 455101.
80. J. H. Granger, M. C. Granger, M. A. Firpo, S. J. Mulvihill and M. D. Porter, *Analyst*, **2013**, 138, 410.
81. S. Harmsen, R. Huang, M. A. Wall, H. Karabeber, J. M. Samii, M. Spaliviero, J. R. White, S. Monette, R. O'Connor, K. L. Pitter, S. A. Sastra, M. Saborowski, E. C. Holland, S. Singer, K. P. Olive, S. W. Lowe, R. G. Blasberg and M. F. Kircher, *Sci. Transl. Med.*, **2015**, 7, 271ra7.
82. Y. Pang, C. Wang, L. Lu, C. Wang, Z. Sun and R. Xiao, *Biosens. Bioelectron.*, **2019**, 130, 204.
83. T. D. Li, R. Zhang, H. Chen, Z. P. Huang, X. Ye, H. Wang, A. M. Deng and J. L. Kong, *Chem. Sci.*, **2018**, 9, 5372.
84. W. Nam, X. Ren, I. Kim, J. Strobl, M. Agah and W. Zhou, *Anal Chem*, **2021**, 93, 4601.
85. H. Ito, K. Hasegawa, Y. Hasegawa, S. Kimura, M. Onimaru, T. Ohmori, H. Ikeda, M. Saito, Y. Kitamura, C. Sato, K. Gomi, S. Sakaue, M. Isozaki, M. Matsukawa and H. Inoue, *J. Clin. Oncol.*, **2015**, 33.
86. J. B. Phyo, A. Woo, H. J. Yu, K. Lim, B. H. Cho, H. S. Jung and M. Y. Lee, *Anal. Chem.*, **2021**, 93, 3778.
87. L. Litti, A. Ramundo, F. Biscaglia, G. Toffoli, M. Gobbo and M. Meneghetti, *J. Colloid Interface Sci.*, **2019**, 533, 621.
88. S. Bhattacharya, X. Gong, E. Wang, S. K. Dutta, J. R. Caplette, M. Son, F. T. Nguyen, M. S. Strano and D. Mukhopadhyay, *Cancer Res.*, **2019**, 79, 4515.
89. P. T. Sujai, S. Shamjith, M. M. Joseph and K. K. Maiti, *ACS Appl. Bio. Mater.*, **2021**, 4, 4962.
90. B. Y. Zhang, P. Yin, Y. Hu, C. Szydzik, M. W. Khan, K. Xu, P. Thurgood, N. Mahmood, C. Dekiwadia, S. Afrin, Y. Yang, Q. Ma, C. F. McConville, K. Khoshmanesh, A. Mitchell, B. Hu, S. Baratchi and J. Z. Ou, *Biosens. Bioelectron.*, **2022**, 198, 113814.
91. X.-S. Zheng, I. J. Jahn, K. Weber, D. Cialla-May and J. Popp, *Spectrochim. Acta, Part A*, **2018**, 197, 56.
92. U. Parlatan, M. O. Ozen, I. Kecoglu, B. Koyuncu, H. Torun, D. Khalafkhany, I. Loc, M. G. Ogut, F. Inci, D. Akin, I. Solaroglu, N. Ozoren, M. B. Unlu and U. Demirci, *Small*, **2023**, 19, 2205519.

93. M. Peng, Z. Wang, X. Sun, X. Guo, H. Wang, R. Li, Q. Liu, M. Chen and X. Chen, *Anal Chem*, **2022**, 94, 11483.
94. W. Dawuti, J. Dou, J. Li, R. Zhang, J. Zhou, M. Maimaitiaili, R. Zhou, R. Lin and G. Lü, *Photodiagn. Photodyn. Ther.*, **2023**, 42, 103544.
95. W. Li, L. Xiong, N. Li, S. Pang, G. Xu, C. Yi, Z. Wang, G. Gu, K. Li, W. Li, L. Wei, G. Li, C. Yang and M. Chen, *J. Mater. Chem. C*, **2019**, 7, 10179.
96. J. I. Varillas, J. Zhang, K. Chen, I. I. Barnes, C. Liu, T. J. George and Z. H. Fan, *Theranostics*, **2019**, 9, 1417.
97. R. Kalluri and V. S. LeBleu, *Science*, **2020**, 367.
98. N. Cheng, D. Du, X. Wang, D. Liu, W. Xu, Y. Luo and Y. Lin, *Trends Biotechnol.*, **2019**, 37, 1236.
99. S. Nagrath, L. V. Sequist, S. Maheswaran, D. W. Bell, D. Irimia, L. Ulkus, M. R. Smith, E. L. Kwak, S. Digumarthy, A. Muzikansky, P. Ryan, U. J. Balis, R. G. Tompkins, D. A. Haber and M. Toner, *Nature*, **2007**, 450, 1235.
100. Y. Wen, V. X. Truong and M. Li, *Nano Lett.*, **2021**, 21, 3066.
101. H. Karabeber, R. Huang, P. Iacono, J. M. Samii, K. Pitter, E. C. Holland and M. F. Kircher, *ACS Nano*, **2014**, 8, 9755.
102. S. Harmsen, S. Rogalla, R. Huang, M. Spaliviero, V. Neuschmelting, Y. Hayakawa, Y. Lee, Y. Tailor, R. Toledo-Crow, J. W. Kang, J. M. Samii, H. Karabeber, R. M. Davis, J. R. White, M. van de Rijn, S. S. Gambhir, C. H. Contag, T. C. Wang and M. F. Kircher, *ACS Nano*, **2019**, 13, 1354.
103. L. M. Almond, J. Hutchings, G. Lloyd, H. Barr, N. Shepherd, J. Day, O. Stevens, S. Sanders, M. Wadley, N. Stone and C. Kendall, *Gastrointes. Endosc.*, **2014**, 79, 37.
104. S. P. Misra, M. Dwivedi and K. Sharma, *Endoscopy*, **2011**, 43, 985.